The Influences of Boundary Layer Parameterization Schemes on Mesoscale Heavy Rain System①

Xu Liren (许丽人) and Zhao Ming (赵 鸣)

Department of Atmospheric Sciences, Nanjing University, Nanjing 210093

(Received September 10, 1999; revised March 6, 2000)

ABSTRACT

The mesoscale numerical weather prediction model (MM4) in which the computations of the turbulent exchange coefficient in the boundary layer and surface fluxes are improved, is used to study the influences of boundary layer parameterization schemes on the predictive results of the mesoscale model. Seven different experiment schemes (including the original MM4 model) designed in this paper are tested by the observational data of several heavy rain cases so as to find an improved boundary layer parameterization scheme in the mesoscale meteorological model. The results show that all the seven different boundary layer parameterization schemes have some influences on the forecasts of precipitation intensity, distribution of rain area, vertical velocity, vorticity and divergence fields, and the improved schemes in this paper can improve the precipitation forecast.

Key words: Boundary layer parameterization, Mesoscale numerical weather prediction (MNWP), Turbulent exchange coefficient, Surface fluxes, Heavy rain

1. Introduction

The mesoscale operational model, which is often used, is MM4 or MM5, but MM4 is used frequently on 10^3 km scale. The physical processes in this model develop constantly. For original MM4, the computation of surface fluxes is not accurate, and K model for the turbulence fluxes between any 2 levels needs to be improved by new treatment. In order to study the influences of boundary layer parameterization schemes on mesoscale heavy rain system, surface fluxes and K model in original MM4 are improved by the recent research in this paper. The flux–profile relations for various stability conditions are employed in the computation of surface fluxes, and K model is designed as follows: 1) Mellor–Yamada level 2.5 model, in which the prognostic equation of turbulent kinetic energy (TKE) is introduced, but ε is diagnostic; 2) E–ε model, for which, kinetic energy (E), viscous dissipation (ε) are all prognostic; 3) E–ε–l model, in which a diagnostic mixing length (l) is added in E–ε model. In this paper some heavy rain cases in the Yangtze River and the Huaihe River basins are used to test the model. Experiments show that the prediction of heavy rain with improved schemes in this paper is better than the results of original MM4. So it is necessary to improve boundary layer parameterizations in the MM4 model. In addition, it is feasible that schemes designed in this paper can also be used in the mesoscale model MM5.

①This paper was supported by the National Natural Science Foundation of China (Grant No. 49875005 and No. 49735180).

2. Model description and observational data

2.1 *Bulk boundary layer parameterization scheme*

This is a kind of original MM4 scheme, in which various fluxes are derived by the product of the drag coefficient and the difference of meteorological elements between the surface and atmosphere, and the turbulent exchange coefficient K is computed by the traditional K model (Blackadar K model). This scheme is used to compare with new schemes. Details may be found in Anthes and Kuo (1987).

2.2 *Improved MM4 boundary layer parameterization schemes*

2.2.1 *Improved surface fluxes algorithm*

For new profile–flux relationship under various stability conditions (Zeng et al., 1998), the stability is classified into five types: very unstable, unstable, neutral, stable and very stable. Here, the flux–gradient relations under very stable condition are obtained with $\varphi_m = \varphi_h = 5 + \zeta$; those under very unstable condition are obtained with $\varphi_m = 0.7\kappa^{2/3}(-\zeta)^{1/3}$ and $\varphi_h = 0.9\kappa^{4/3}(-\zeta)^{-1/3}$, where φ_m and φ_h represent dimensionless wind and temperature shears respectively, κ is the Von Karman constant, $\zeta = \frac{z}{L}$, L is the Monin–Obukhov length; the Businger–Dyer relation is used for other stability conditions. The surface fluxes are obtained from the winds, temperatures and moistures at the lowest level of the model and surface with iterative algorithm by above flux–gradient relations, and this scheme is not used in the mesoscale model at present. In addition, scalar roughness is calculated in this scheme, and it is given by friction velocity (u_*) and roughness. Some researches show that it cannot be ignored (Ren et al., 1999).

2.2.2 *Turbulence closure scheme*

2.2.2.1 *Level 2.5 turbulence closure scheme*

In the higher–order closure, if the prognostic equation of turbulent kinetic energy q^2 (twice of actual turbulent kinetic energy) is reserved, the other turbulence items are expressed by algebra equations connected with q^2, we call this kind of closure as level 2.5 turbulence closure scheme (Mellor and Yamada, 1982), that is

$$-\overline{wu} = K_M \partial U / \partial z \quad , \tag{2.1}$$

$$-\overline{wv} = K_M \partial V / \partial z \quad , \tag{2.2}$$

$$-\overline{w\theta} = K_H \partial \theta / \partial z \quad , \tag{2.3}$$

$$K_M = lqS_M \quad , \tag{2.4}$$

$$K_H = lqS_H \quad , \tag{2.5}$$

$$\frac{Dq^2}{Dt} - \frac{\partial}{\partial z}\left[lqs_q \frac{\partial q^2}{\partial z}\right] = -2\overline{wu}\frac{\partial U}{\partial z} - 2\overline{wv}\frac{\partial V}{\partial z} + 2\beta g\overline{w\theta} - 2\varepsilon \quad , \tag{2.6}$$

$$q^2 = \overline{u}^2 + \overline{v}^2 + \overline{w}^2 \quad , \tag{2.7}$$

$$\varepsilon = q^3 / \Lambda_1 \quad , \tag{2.8}$$

where l is the mixing length, ε is the rate of viscous dissipation, Λ_1 is the length scale, $S_q = 0.2$, Λ_1 and the expressions of S_M, S_H are seen in Mellor and Yamada (1982).

At the model bottom $q^2 = B_1^{2/3} u_*^2$, B_1 was given in Mellor and Yamada (1982); the upper boundary layer condition is $q^2 = 0$. In the vertical coordinate, q^2 is located at full σ levels of MM4.

2.2.2.2 *E–ε turbulence closure scheme*

In the E–ε turbulence model, the eddy–exchange coefficient is evaluated from the turbulent kinetic energy (E) and the dissipation rate (ε) of turbulent kinetic energy, here E and ε are all predicted. Lee and Kao (1979) firstly used the E–ε model in the questions of atmospheric boundary layer (ABL), and derived the eddy–exchange coefficient. Mason and Sykes (1980) studied the dynamics of large–scale, horizontal roll vortices in the neutral ABL with an E–ε model. Detering and Etling (1985a) employed the E–ε model in the PBL model, and (1985b) studied its application in mesoscale atmospheric flows, especially studied boundary layer; Duynkerke et al. (1987) studied turbulent structure of the stratocumulus–topped ABL, and the neutral and stable atmospheric boundary layer by E–ε model (Duynkerke, 1988). Gerber et al. (1989) studied a marine boundary layer jet with E–ε model. Using E–ε model, Ly (1991) studied coupled air–sea boundary layer structure, and Alapaty et al. (1994) simulated monsoon boundary layer processes in a regional scale nested model. But E–ε model has not been applied to MM4 system yet. Since ε is derived by prognostic equation, it is an improvement over the level 2.5 model.

In E–ε model, E, ε are given by

$$K = c_k \frac{E^2}{\varepsilon} , \tag{2.9}$$

$$\frac{dE}{dt} - \frac{\partial}{\partial z}[\alpha_e K \frac{\partial E}{\partial z}] = K[(\frac{\partial U}{\partial z})^2 + (\frac{\partial V}{\partial z})^2 - \frac{g}{\theta}\frac{\partial \theta}{\partial z}] - \varepsilon , \tag{2.10}$$

$$E = \frac{1}{2}(\overline{u}^2 + \overline{v}^2 + \overline{w}^2) , \tag{2.11}$$

$$\frac{d\varepsilon}{dt} - \frac{\partial}{\partial z}[\alpha_\varepsilon K \frac{\partial \varepsilon}{\partial z}] = \frac{c_1 \varepsilon}{E}\{K[(\frac{\partial U}{\partial z})^2 + (\frac{\partial V}{\partial z})^2]\} - c_2 \frac{\varepsilon^2}{E} , \tag{2.12}$$

where $c_k = 0.033$, $c_1 = 1.44$, $c_2 = 1.92$, $\alpha_e = 1.0$ and $\alpha_\varepsilon = 0.77$.

At the model bottom: $\begin{cases} E = c_k^{-1/2} u_*^2 \\ \varepsilon = u_*^3 \left\{ \dfrac{\varphi_m}{\kappa z_0} - \dfrac{1}{\kappa L} \right\} \end{cases}$, and at the model top: $E = 0$; $\varepsilon = 0$.

Here φ_m is the dimensionless wind shear function, and corresponding to the five stability conditions in Section 2.2.1 (see Zeng et al., 1998). ε is also deposited at full σ levels of MM4.

2.2.2.3 *E–ε–l turbulence closure scheme*

Xu and Taylor (1997) studied the E–ε–l closure scheme in order to improve the E–ε closure scheme of boundary layer. They studied only neutrally stratified case. In this paper, it is extended to stable and unstable conditions and is applied to the mesoscale model.

For E–ε–l closure, TKE closure is still used for K concerning with E and l_m. The expression of l_m in the classical boundary theory is used. ε is not diagnostic but prognostic so as

to compute E accurately. The equations include prognostic equations of E and ε. K_m is expressed as

$$K_m = (\alpha E)^{1/2} l_m \ . \tag{2.13}$$

The mathematical expression for l_m is

$$l_m^{-1} = \frac{1}{\kappa(z + z_0)} + \frac{1}{\lambda} \ , \tag{2.14}$$

where $\lambda = 0.0063u_* / f$, $\alpha = 0.3$. The $E-\varepsilon-l$ scheme has not been used in the mesoscale model currently.

2.3 *Experiment design*

According to the above principles, we designed seven experiment schemes:

Test 1: Surface fluxes of bulk aerodynamic algorithms and K model of original MM4 are used, which is control experiment and used to compare;

Test 2: K is computed by level 2.5 turbulence closure scheme, surface fluxes use bulk flux algorithm;

Test 3: K is computed by $E-\varepsilon$ turbulence closure scheme, surface fluxes use bulk flux algorithm;

Test 4: K is computed by $E-\varepsilon-l$ turbulence closure scheme, surface fluxes use bulk flux algorithm;

Test 5: K is computed by level 2.5 turbulence closure scheme, surface fluxes use the profile–flux relations under various stability conditions;

Test 6: K is computed by $E-\varepsilon$ turbulence closure scheme, surface fluxes use the profile–flux relations under various stability conditions;

Test 7: K is computed by $E-\varepsilon-l$ turbulence closure scheme, surface fluxes use the profile–flux relations under various stability conditions.

2.4 *Observational data*

In this paper, some cases of heavy rain in the Yangtze River and the Huaihe River basins are analyzed, we focus on analyzing the following three samples:

Case 1: From 0000UTC 12 June to 0000UTC 13 June 1991, the model is integrated for 24 h;

Case 2: From 0000UTC 24 May to 1200UTC 25 May 1991, the model is integrated for 36 h;

Case 3: From 1200UTC 30 June to 0000UTC 2 July 1998, the model is integrated for 36 h.

3. Experiments and analysis

3.1 *Some parameters for MM4 system*

The numerical model employed in this study is the Penn State / NCAR mesoscale model (MM4) described by Anthes et al. (1987). It is a three–dimensional, hydrostatic, primitive–equation model with the terrain–following σ coordinate in the vertical, where $\sigma = \frac{p - p_t}{p_s - p_t}$, and the total of 16 levels is taken, that is, $\sigma = 0.0, 0.1, 0.2, 0.3, 0.4, 0.5, 0.6,$

0.7, 0.78, 0.85, 0.89, 0.92, 0.95, 0.97, 0.99, 1.0. There are $40 \times 41 \times 15$ grids with a horizontal resolution of 60 km. The central point is (36°N, 117°E). Physical parameterizations include the parameterization of planetary boundary layer and surface fluxes, cumulus convection parameterization described by Anthes, and large-scale precipitation parameterization.

3.2 *Comparison of synoptic situations from different schemes*

There was a typical Meiyu in the Yangtze River and the Huaihe River basins between 0000UTC 12 June and 0000UTC 13 June, 1991, when a very heavy rain occurred in the Yangtze River and the Huaihe River basins, causing large-area rain-band with the east-west direction. The observed 24-h maximum precipitation was 172 mm. For this case, the model is integrated for 24 h with the above-mentioned schemes, and results show that only small difference exists among these schemes for 24-h predictive pressure fields. If we increase the integral time, we can find that the difference of synoptic situations increases, but synoptic situations are similar on the whole (figure not shown). The schemes which surface fluxes and K are all changed (tests 5, 6, 7) have slightly greater influence on the situations than those which only K is changed (tests 2, 3, 4), and the formers are closer to observations. This shows that if the integral time is short, the influence of the boundary layer is small, and with the increasing of the integral time, the difference of short-term predicted synoptic situations for different schemes will increase. The reason is that when the integral time increases, the external force increases, too, the effect of boundary is becoming obvious gradually, which is similar to the results from Chen et al. (1995).

The 12-h and 24-h predictive temperature fields from the seven schemes are close to the observed fields, and only small difference exists among these schemes. Temperatures predicted by tests 5-7 are slightly higher than that by test 1 and closer to observations. The reason is that the improvements on surface fluxes for tests 5, 6, 7 have some influence on temperature.

For 12-h predictive flow fields at 850 hPa, the difference among different schemes is not obvious. When the 24-h forecast is at 0000UTC 13 June, convergence appears near (33°N, 117°E) for all these schemes. The intensities of convergence for test 5, test 6, test 7 are stronger than those for tests 1-4. However test 7 has a strong vorticity center here, which corresponds to rain area very well.

3.3 *Comparison of precipitation*

Fig. 1a shows the observed precipitation between 0000UTC 12 June and 0000UTC 13 June, 1991, Figs. 1b-h illustrate the 24-h precipitation forecasted by tests 1-7, respectively. The figures show that: The forecast results from Figs. 1c-h are better than that from Fig. 1b, which means that the distribution of rain area and rainfall intensity predicted by these improved schemes are more consistent with observational results than the original scheme (test 1). This fact shows that the improvement of these schemes is available. The results predicted by test 2 (maximum rainfall of 100 mm), test 3 (maximum rainfall of 109 mm) and test 4 (maximum rainfall of 101 mm) are in better agreement with observations than test 1 (maximum rainfall of 93.2 mm), however comparing test 4 with test 3, the position of the heavy rain center from test 4 is closer to the observations, i.e., three centers are predicted, but the intensity is smaller than that from test 3. The results show that the improvement of the exchange coefficient K in the boundary layer for E-ε model is better than that in E-ε-l and level 2.5 models for the maximum precipitation, nevertheless, E-ε-l model is better than E-ε model for the prediction of the precipitation center position. After considering the improved

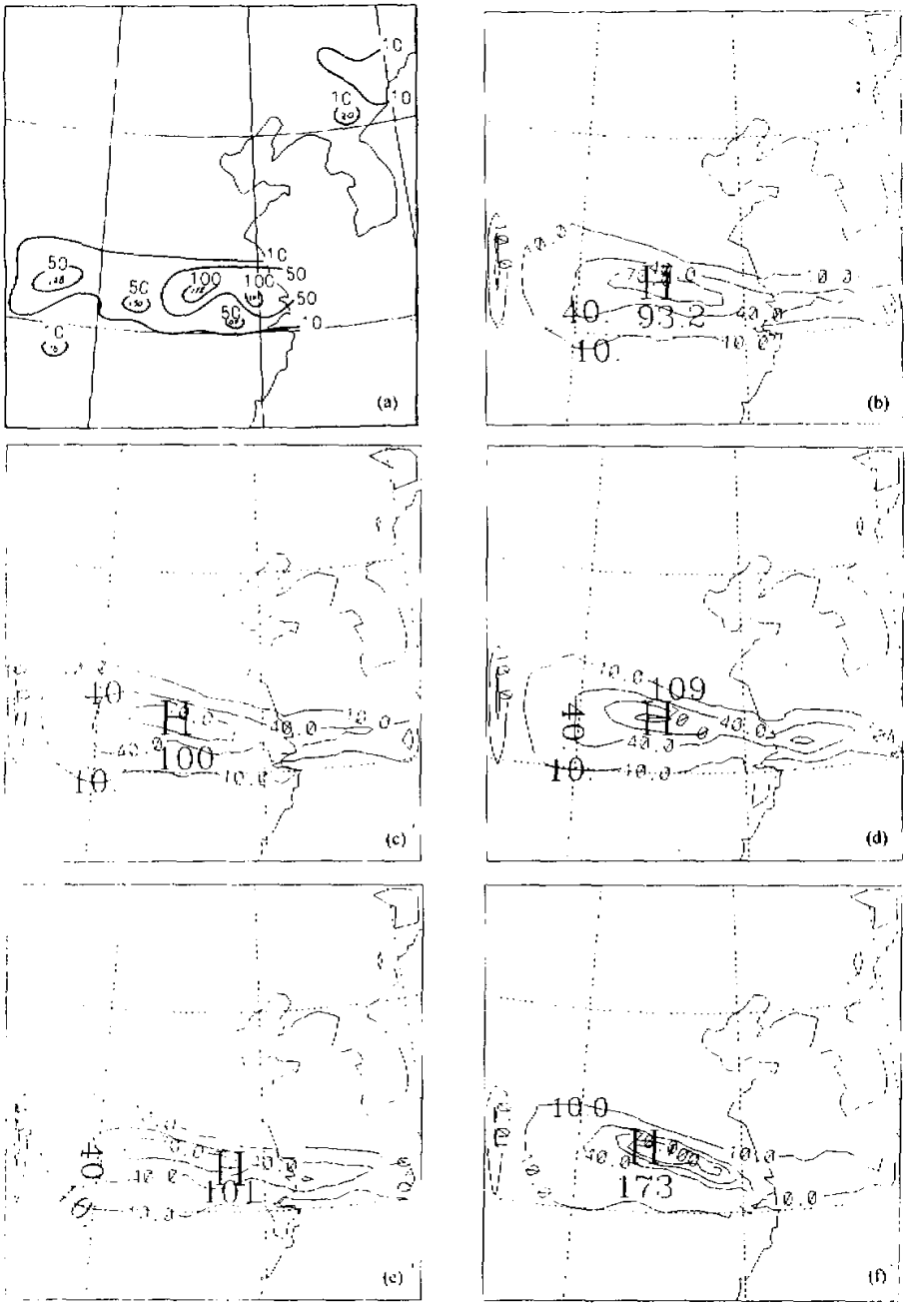
(a)
(b)
(c)
(d)
(e)
(f)

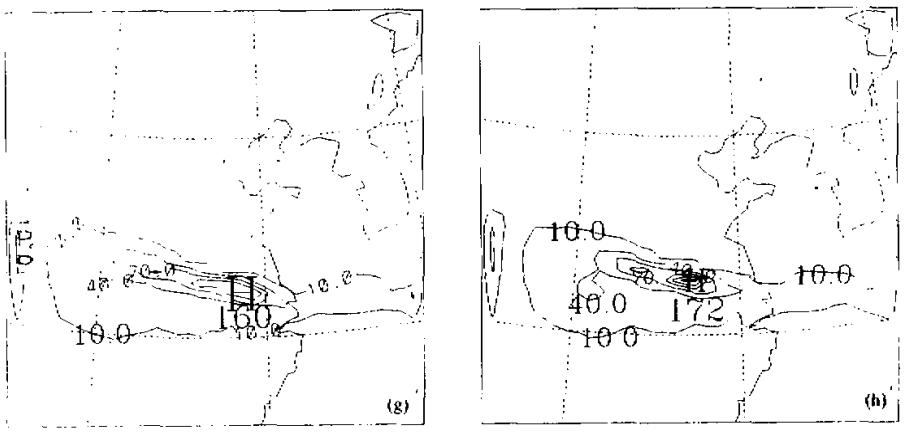

Fig. 1. 24-h precipitation (mm) between 0000UTC 12 June and 0000UTC 13 June, 1991. (a) Observed 24-h precipitation, (b)–(h) Forecasted 24-h precipitation for test 1 (b), test 2 (c), test 3 (d), test 4 (e), test 5 (f), test 6 (g) and test 7 (h).

computation of surface fluxes, test 7 is better than test 5 (maximum rainfall of 112 mm) and test 6 (maximum rainfall of 160 mm), in which the maximum precipitation in 24-h is 172 mm, meanwhile the position of precipitation center is close to observed one. The 24-h precipitation forecasts from test 5 and test 6 are also close to the observations, but the forecasts of corresponding precipitation center positions are not good enough. On the whole, test 5, test 6 and test 7 produce a better precipitation forecast than that in tests 2,3 and 4. This shows that the improvement of surface fluxes has some influence on rainfall. In other words, in the physical process of boundary layer, not only the exchange coefficient has an influence on rainfall, but the influence of surface fluxes cannot be ignored. Combining the influences of the two factors results in that the forecast from test 7 is the best one. Some physical quantities will be analyzed in the following in order to explain the reasons of the influence of boundary layer parameterization on precipitation.

3.4 *Analysis of factors influencing precipitation for Case 1*

3.4.1 *Vertical velocity field*

From the vertical velocity fields at 700 hPa and 850 hPa, we can see that there is close corresponding relations between vertical velocity (ω) and precipitation. Near the area with strong vertical upward motion, there is abundant precipitation on the surface, that is, strong upward motion exists in the heavy rain area. The vertical upward velocity is intensified rapidly from 850 hPa to 700 hPa and results in very strong upward flow in the middle level, which provides a favorable condition to the genesis and evolution of heavy rain. In general, the vapour source of heavy rain mainly depends on the advective transfer and convergence of sufficient vapour in the middle and lower levels (especially in the boundary layer). The convergence of lower air current and divergence of upper air current cause the very strong upward motion in the heavy rain area. And, the heavy rain cluster occurs just near the center of maximum upward motion, resulting in strong precipitation. The greater the vertical up-

ward velocity is, the stronger the precipitation is.

We can see from the computation of vertical velocity fields (figure not shown) that the vicinity of vertical upward velocity area at 700 hPa corresponds to rain area on the surface very well. The distributions of the vertical upward velocity from tests 3, 4, 5, 6 and 7 all take the form of band, corresponding to the banded rain area on the surface. The intensities of vertical upward motion predicted by tests 5, 6 and 7 are far larger than those by test 1, in which the intensity in test 6 is the maximum with two centers, and test 7 has three centers, corresponding to the three precipitation centers on the surface. Very strong vertical upward velocities exist in the heavy rain area of all schemes. Nevertheless, the precipitation forecast from the scheme with the strongest vertical upward velocity is not the closest to the observations. The reason is that there are many kinds of factors influencing precipitation, and the vertical upward velocity is only one of the dynamic factors.

In addition, the changes of divergence field with time can influence the changes of vertical velocity field with height. When convergence is intensified somewhere, vertical upward motion is also developed. On the contrary, when convergence is weakened or divergence is intensified somewhere, vertical upward motion will be weakened or sinking motion will be strengthened. Before or after heavy rain cluster occurs, the changes of the divergence in lower level with time are very great. When the changes of divergence with time are small, vertical upward motion cannot develop so that the mesoscale low is weakened and filled up quickly. Obviously, it is impossible to cause the activity of heavy rain cluster. The relation between the allocation of divergence field in lower and upper levels and severe rain cluster decides the characteristics of vertical motion. If there is only convergence in lower level, but not divergence in upper level, consequentially the surface pressure is strengthened, the mesoscale low is filled up quickly, thereby convergence in lower level stops. Only under the conditions that convergence in lower level matches divergence in upper level and the total divergence is greater than the total convergence, the surface pressure is weakened sequentially, convergence in lower level is further strengthened, then vertical upward motion can develop and maintain. From the horizontal and vertical cross-section diagram of the divergence field (figure not shown), we can see that strong convergence center and negative divergence area at 850 hPa correspond to the surface rain area. There are convergence centers at 700 hPa, too. At 500 hPa the intensity of convergence center is weakened. However it turns to divergent flow field at 200 hPa. Comparing divergence of test 7 with that of test 1, the intensity of convergence center in test 7 is stronger than that in test 1, the relation between negative divergence area and rain-band is better than that in test 1, the results from test 7 are more consistent with observations. Therefore it can be obtained that the appearance of the strong convergence center in the boundary layer and the formation and maintenance of intense pumping are important conditions of the genesis and development of heavy rain cluster.

3.4.2 *Analysis of vorticity field*

From 12-h predicted voticity fields at 850 hPa (figure not shown), we see that the slightly southern area under the center of strong positive vorticity fields at 850 hPa corresponds to the rain area, and the rain area center is close to the positive vorticity center. It may be seen from the vertical cross-section diagram (figure not shown) of vorticity that there is positive vorticity area below 500 hPa in the heavy rain area, while corresponding divergence field is convergent, however it becomes negative vorticity area above 500 hPa. The vertical distribution of vorticity is just reverse in the rainless area. Comparison of convergence fields

between 12–h forecast and 24–h forecast shows that during this heavy rain event, positive vorticity moves eastward and is strengthened gradually, at the same time divergence field is convergent. It has been verified with experiments that convergence plays a predominant role in the genesis and development of vorticity (The group of meso and small scale test base heavy rain in the middle of Hunan Province, 1988). The increase of positive vorticity demonstrates that the genesis and development of cyclonic circulation are favorable for the movement of mesoscale low and heavy rain cluster. The distribution of positive vorticity is closely related to the distribution of heavy rain area. Comparison of different schemes shows that test 7 is the best scheme, there are the best correspondence relations between vorticity field distribution, strong vorticity center and the distribution of heavy rain and precipitation center. Vorticity fields predicted by tests 2–7 are all more consistent with observations than that by the original model. It is proved that the improvements of the boundary layer scheme make the vorticity field be improved, further influence precipitation and cause the difference of precipitation forecast, which shows that the vorticity is one of the important dynamic factors influencing precipitation, too.

3.4.3 *Low level jet (LLJ)*

Commonly, the low level jet (LLJ) is considered as the most important factor supplying vapour and momentum to mid–latitude heavy rain and severe storm. The trigger action of low level jet to heavy rain was studied from dynamic point of view. Uccellini et al. and Wang Jizhi (see Zheng, 1989) explained the allocation relations between heavy rain and upper and low level jets by discussing the adjustment between mass and momentum fields connected with upper and low level jets, and presented a viewpoint that the coupling of upper and low level jets might trigger and maintain the heavy rain mesoscale convective system. It can be found from comparison of LLJs from different schemes that the southwestern–northeastern LLJ existed at 700 hPa at 1200UTC 12 June for these schemes and heavy rain appeared in left front of the LLJ maximum velocity area and the right back of upper level jet. Figs. 2a, b depict the 24–h predicted LLJ at 850 hPa. We analyzed the 12–h predicted LLJ (figure not shown), too. For these schemes, the LLJ appeared at 700 hPa at 1200UTC 12 June, and differences among these schemes are not obvious. But for 24–h forecast (at 0000UTC 13 June), LLJ is strengthened, and differences among these schemes are more obvious. LLJ from these improved schemes is more obvious than that from test 1. LLJ from test 7 is the strongest and has the closest relationship with the rain area. The stronger LLJ is, the wider the scopes of the corresponding heavy rain area are and the stronger the intensity is. The reason is that the strong or weak degree of jet reflects approximately the accumulative degree of kinetic energy. The stronger the jet is, the more kinetic energy accumulates and the more obvious its dynamic effect is. These are even more favorable for the genesis of heavy rain. In addition, the changes of LLJ intensity have a close relationship with heavy rain. LLJ is strengthened continually in the process of 24–h forecast. But it has been found that primary precipitation sometimes appears after LLJ is strengthened. Fig. 3 depicts the vertical cross–section diagram of the 24–h predicted low level jet, which is the south–north cross–section passing the point (14,20). It may be seen from analysis that there exists a LLJ in test 7, and the maximum velocity may reach 18 m/s at 850 hPa. Except the forecast error from MM4 itself, the results from test 6 and test 7 are closer to observations, and the results from these improved schemes are in better agreement with observations than that from test 1. It is found from vertical cross–section

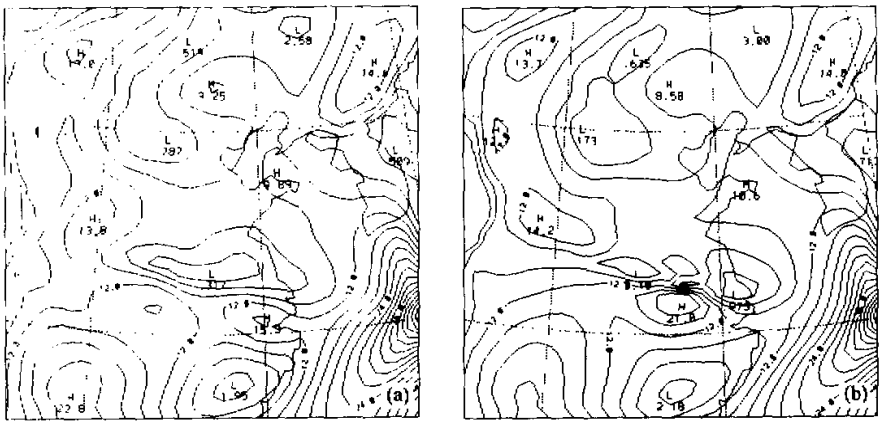

Fig. 2. 24-h predicted low-level jet (LLJ) (m / s) at 850 hPa for test 1 (a) and for test 7 (b).

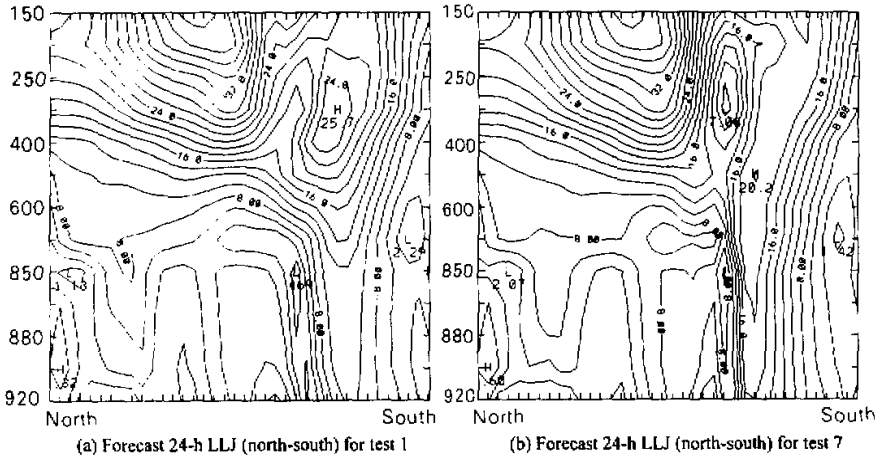

Fig. 3. Vertical cross-section diagram of the 24-h predicted LLJ (m / s) passing (14,20). (a) for test 1, (b) for test 7.

diagrams of vorticity, divergence and vertical velocity (figure not shown) that the left of low level jet is convergent (negative divergence) area with positive vorticity and upward motion. The right of LLJ is divergent (positive divergence) area with negative vorticity and downward motion predominates. The three centers, i.e., positive vorticity center, convergence center and maximum upward motion center, are close to each other. The precipitation during this heavy rain event appears primarily in this region. The above analysis shows that low level jet is a warm and moist flow with high speed, it not only is important channel of vapour transfer, but also produces the convergence of a great deal of vapour on the left of jet. At the same time it assures the supply of unstable energy. There are strong convergence and upward motion on its left, potential unstable energy got released, and the convective motion occurred and devel-

oped. The genesis and evolution of convective motion promote the maintenance and strength of low level jet. The maintenance of low level jet assures the supply and complement of vapour and unstable energy. Such and such, until the characteristics are changed and LLJ is weakened and disappears with the weakness and cease of convective motion. Then the heavy rain event is over. Even though the atmospheric stratifications in the middle and lower levels on the right of LLJ are still potential unstable, because corresponding motion is divergent and sinking, suppressing the release of potential unstable energy. It is not favorable for the evolution of convective motion. LLJ, heavy rain and other intense convective weather make up some allocation relation due to the thermal and dynamic characteristics of LLJ. Thus LLJ is also a very important dynamic factor influencing precipitation.

3.4.4 *Comparison of* θ_{se}

Air is always in motional state. Its state parameters (such as: temperature, pressure and humidity) also keep varying. However, there are some characteristic quantities, such as potential pseudo-equivalent temperature, which is invariable with air parcel motion. Figures 4 and 5 show the profiles of θ_{se} passing the point (14, 21) (in the rain area) from test 1 and test 7, respectively. Curve A is a profile of θ_{se} at the initial time, and curve B is the 12-h predicted θ_{se}. $\frac{\partial \theta_{se}}{\partial z} < 0$ is usually considered as a potential instability criterion. From the profiles of θ_{se} between 850 hPa and 500 hPa in Fig. 4 and Fig. 5, it is seen that θ_{se} decreases with the increase of height under 500 hPa. This shows that atmosphere in middle and lower levels of the troposphere is potential unstable. It can be seen from comparison of the two figures that the reduction of θ_{se} under 500 hPa with the increase of height from test 7 was faster than that from test 1 at 1200UTC 12 June. This shows that atmospheric stratification is more unstable for test 7. Point (14,21) lies on the left of LLJ and is close to the rain area center. An upward motion area corresponding to strong convergence is located on the left of LLJ where potential unstable energy is released, and it is favorable for the development of convective activity and the genesis and evolution of heavy rain.

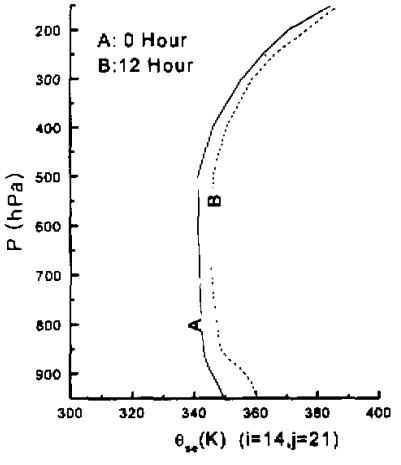

Fig. 4. θ_{se} profile passing (14,21) for test 1 (K).

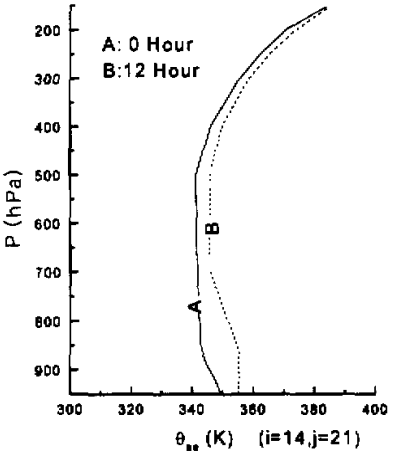

Fig. 5. θ_{se} profile passing (14,21) for test 7 (K).

Based on the above analysis, the improvement of boundary layer schemes influences the distribution of heavy rain and precipitation intensity by influencing many factors including vorticity, divergence, low level jet, vertical motion velocity and θ_{se}. Studies show that test 7 is most successful in simulating heavy rain from 0000UTC 12 June to 0000UTC 13 June 1991. For this case, the forecast by the original scheme is good, then the improvement of boundary layer parameterizations makes heavy rain forecast more accurate. For the cases with unsuccessful precipitation forecasts by the original scheme, the results from these improved schemes in this paper are not good enough, too. This shows that boundary layer processes depend extremely on the dynamic frame of the mesoscale model. Therefore, dynamic processes are primary factors influencing heavy rain. As for the boundary layer process, it makes heavy rain forecast more exact on the basis of better dynamic frame. Obviously, the influence of the boundary layer cannot be neglected.

3.5 *Case 2 analysis*

The case of 0000UTC 24 May–1200UTC 25 May 1991 is simulated by these schemes. The model is integrated for 36 h. This case is a heavy rain during the beginning of the Meiyu period, which is convective weather with the strong Meiyu front. There was a great deal of precipitation throughout the country in the period of 1200UTC 24 May–1200UTC 25 May, and the rain area extended all over North China, middle China and East China. But the heavy precipitation distributed primarily in the Yangtze River and the Huaihe River basins. The maximum observed 24–h precipitation was 173 mm.

It is found throughout comparison of synoptic situations that there is small difference between tests 2, 3, 4 and the original scheme. This kind of difference is more obvious than 24–h forecast of case 1, and there is greater difference between tests 5, 6, 7 and the original scheme. Except for the forecast error from MM4 itself, the results from test 5, test 6 and test 7 are closer to observations. This shows that the difference of synoptic situations will increase with the increase of integral time. Conclusions are analogous to case 1.

The comparison of precipitation is described in the following table. Table 1 shows the predicted maximum precipitation between 1200UTC 24 May and 1200UTC 25 May.

Table 1. Comparison of forecast of maximum precipitation among different schemes

	Forecast (mm)	Observation (mm)
Test 1	251	173
Test 2	246	173
Test 3	198	173
Test 4	238	173
Test 5	225	173
Test 6	178	173
Test 7	193	173

For the maximum precipitation, the result from test 6 is the closest to the observations. But from predicted 24–h precipitation figures, combining both the distribution of rain area and center position, the results of test 7 are better than test 6. The conclusion that the position of precipitation center forecasted by test 7 is very good is mentioned in case 1. Test 7 is superior to test 6 from this viewpoint. In general, the precipitation forecasts from tests 2–7 are closer to the observations than the original scheme. We can see by reviewing case 1 that the

predicted precipitation by improved surface fluxes algorithms is greater than that by the original scheme (test 1). In this case the predicted precipitation by improved surface fluxes algorithms is smaller than that by the original scheme. The results from the two cases are all closer to the observations. This shows that the improvement of surface fluxes is valid to precipitation forecast.

Conclusions resulting from the analyses of vorticity, divergence, vertical velocity and low level jet are analogous to case 1. Characteristics of vorticity, divergence, vertical upward velocity, low level jet at 850 hPa and rain area distribution are analogous to case 1. These improved schemes can simulate LLJ well, the results are closer to the observations, and the structures of LLJ are similar to case 1.

It is worth noting that the results from tests 6 and 7 are all good for the above two cases. Sometimes the result of test 6 is better than that of test 7, the reason is that the difference between E–ε–l closure scheme and E–ε closure scheme is small, although E–ε–l is more perfect than E–ε model in theory, the results are complicated due to the complexity of affecting factors in the real atmosphere. It is sure that the results of E–ε–l method and E–ε method are better than the original scheme, even than level 2.5 method after improving exchange coefficient K of boundary layer parameterization.

3.6 *Case 3 analysis*

Case 3 is from 1200UTC 30 June to 0000UTC 2 July 1998. The models are integrated for 36 h. The observed precipitation between 0000UTC 1 July and 0000UTC 2 July was located in a northeast–southwest banded rain area along the line Xiangfan–Kaifeng–Jinan, and the 24–h maximum precipitation was 145 mm.

In this case, we focus on the comparison between test 1 and test 7. The conclusions from this case are analogous to case 1 and case 2. The distributions of rain area forecasted by the two schemes are close to observations. The maximum precipitation simulated by test 7 is closer to observations than by test 1, which is 74.0 mm for test 7, but 66.6 mm for test 1. Although predicted precipitation intensities are all weak, test 7 is still better than test 1, because of its 11.1% improved rainfall forecast from boundary layer parameterization. This magnitude is rational basically.

4. Summary and conclusions

From the forecast of several heavy rain processes in the Yangtze River and the Huaihe River basins by the above seven schemes we see that there are differences of forecasts on precipitation intensity and rain area distribution among different boundary layer parameterizations. In general, the results from the improved boundary layer parameterization schemes with the improvements of either exchange coefficient K or surface fluxes, are closer to the observations than the original scheme. On the improvement of exchange coefficient K, the schemes in which both E and ε are prognostic are more rational than the schemes in which only E is prognostic, but ε is diagnostic, and the forecast is also better for the former than for the latter. After the surface fluxes algorithm is improved, the scheme with E–ε–l turbulence closure and new surface flux algorithm is the most perfect in theory. Summing up forecast results from several tests, test 7 is better than other schemes and can reflect truly the influence of boundary layer process on the circulation pattern and precipitation during the short–range heavy rain event. Whether test 7 is the best scheme in other mesoscale models or not, the conclusion is uncertain in this paper. It needs to be tested by a lot of exper-

iments. The simulated cases in this paper are the cases that successful mesoscale forecasts have been produced with the original scheme. The cases that the difference between results forecasted by the original scheme and observations is rather great were simulated by tests 2–7 in this study, too, however, the errors are still great. This explains that the boundary layer process depends strongly upon the mesoscale dynamical frame.

In addition, we also find that the influence of the improvement of boundary layer parameterizations on the forecast of weather pattern field (temperature, pressure) is not obvious in the short-range weather forecast (for example 24-h), but there is much influence on precipitation intensity and rain area distribution. The reason is that different boundary layer processes have an effect on the intensity and structure of various elements, including LLJ, convergence and divergence fields. This shows that precipitation not only depends on synoptic situation, but also the boundary layer plays an important role in the microstructure of precipitation. It can be seen from this research that boundary layer processes are sensitive to short-range weather forecast. Firstly, the lower level atmosphere is influenced obviously, secondly, the upper and wider atmosphere is influenced through turbulence, diffusion and advection process. So the boundary layer process is very important and cannot be neglected in the numerical weather prediction model.

From the improvement of PBL process in the mesoscale model MM4, we not only can research its influence on precipitation but also analyze the microstructure of boundary layer, (for example, wind, temperature profile in boundary layer, E,ε), which will be discussed in another paper.

The present schemes also can be applied to boundary layer parameterizations in MM5. It will be studied in the future.

Thanks are due to Tang Jianping of Nanjing University for his help in this paper.

REFERENCES

Alapaty K., Sethu Raman, and R.V. Madala, 1994: Simulation of monsoon boundary layer processes using a regional scale nested grid model. *Bound. Layer Meteor.*, **67**, 407–426.

Anthes, R. A., and Y. H. Kuo, 1987: *Description the Penn State/ NCAR Mesoscale Model Version 4 (MM4)*. NCAR Tech.Note NCAR / TN-282+STR.

Chen Yuchun, Qian Zhengan et al., 1995: The comparative experiment of influences about surface drag coefficients in boundary process on numerical boundary process on numerical weather forecasting heavy rain. *Plateau Meteorology*, **14**, 434–442 (in Chinese).

Detering, H. W., and D. Etling, 1985a: Application of the E–ε turbulence model to the atmospheric boundary layer. *Bound. Layer Meteor.*, **33**, 113–133.

Detering, H. W., and D. Etling, 1985b: Application of the energy–dissipation turbulence model to mesoscale atmospheric flows. *Seventh Symp. on Turbulence and Diffusion*, Boulder, *Amer. Meteor. Soc.*, 281–284.

Duynkerke, P. G., and A. G. M. Driedonks, 1987: A model for the turbulent structure of the stratocumulus–topped atmospheric boundary layer. *J. Atmos. Sci.*, **44**, 43–64.

Duynkerke, P. G., 1988: Application of the E–ε turbulence closure model to the neutral and stable atmospheric boundary layer. *J. Atmos. Sci.*, **45**, 865–880.

Gerber, H., S. Chang, and T. Holt, 1989: Evolution of a marine boundary layer jet. *J. Atmos. Sci.* **46**, 1312–1326.

Lee, H. N., and S. K. Kao, 1979: Finite–element numerical modeling of atmospheric turbulent boundary layer. *J. Appl. Meteor.*, **18**, 1287–1295.

Ly L. N., 1991: An application of E–ε turbulence model for studying coupled air–sea boundary layer structure. *Bound. Layer Meteor.*, **54**, 327–346.

Mason, P. J., and R. I. Sykes, 1980: A two-dimensional numerical study of horizontal roll vortices in the neutral atmospheric boundary layer. *Quart. J. Roy. Meteor. Soc.*, **106**, 351–366.

Mellor G. L., and Tetsuji Yamada, 1982: Development of a turbulence closure model for geophysical fluid problems. *Reviews of Geophysics and Space Physics*, **20**, 851–875.

Ren Junfang, Su Bingkai, Zhao Ming, 1999: The influences of scalar roughness on earth–atmosphere exchange. *Chinese J. Atmos. Sci.*, **23**, 349–358 (in Chinese).

The group of meso and small scale test base heavy rain in the middle of Hunan Province, 1988: *Analysis and Prediction of Mesoscale Heavy Rain*. Beijing: China Meteorological Press (in Chinese).

Xu Dapeng and Peter A. Taylor, 1997: An E–ε–l turbulence closure scheme for planetary boundary-layer models: The neutrally stratified case. *Bound. Layer Meteor.*, **84**, 247–266.

Zeng Xubin, Ming Zhao, and Robert E. Dickinson, 1998: Intercomparison of bulk aerodynamic algorithms for computation of sea surface fluxes using TOGA COARE and TAO data. *J. Climate*, **11**, 2628–2644.

Zheng Liangjie, 1989: *Diagnostic Analysis and Numerical Simulation of Mesoscale Synoptic System*. Beijing: China Meteorological Press, 189 pp (in Chinese).